5

Frictional Characteristics in Deeper Part of Seismogenic Transition Zones on a Subduction Plate Boundary

Keisuke Ariyoshi and Yoshiyuki Kaneda
Earthquake and Tsunami Research Project for Disaster Prevention, Japan Agency for Marine-Earth Science and Technology, Yokohama, Japan

1. Introduction

By virtue of dense networks of GPS and highly sensitive seismic stations, occurrences of deep low-frequency tremors/earthquakes have been recognized worldwide in the deep portions of subduction plate boundaries (e.g., Schwartz & Rokosky, 2007). Since these tremors and earthquakes have moment release rate smaller than that of regular earthquakes, the low-frequency tremors (LFTs) /earthquakes are classified into "slow-earthquake" group (Ide et al., 2007). The slow-earthquakes occur sometimes independently and sometimes break into chain-reaction propagating at a speed of about 10 km/day. However, a systematic explanation of the origin of such slow-earthquake migrations in some subduction zones is still lacking.

First of this study, we investigate the mechanisms of slow-earthquake migration by comparing observational results and numerical simulation results. Since some LFTs are found to be modulated by Earth tides (e.g., Nakata et al., 2008) and the moment release rate of the slow earthquake group is much smaller than that of regular earthquakes (Ide et al., 2007), they likely have low-stress drop and are sensitive to shear stress perturbations possibly induced by the preseismic slip of nearby megathrust earthquakes.

Second of this study, we propose a new method to detect precursory change around the large asperity prior to a megathrust earthquake, focusing on the spatio-temporal change of migration speed and moment release rate for nearby slow earthquakes. Recently, low-frequency tremors/earthquakes have been also detected in the shallower portion of frictional transition zone on the subduction plate boundaries (Obana & Kodaira, 2009).

Third of this study, we also perform another numerical simulation of shallow low-frequency tremors/earthquakes, comparing with the characteristics of the deep low-frequency tremors/earthquakes and discussing the strategy of Dense Oceanfloor Network System for Earthquakes and Tsunamis (DONET) toward an anticipated Tonankai Earthquake.

2. What makes low-frequency tremors/earthquakes migrate along strike?

In this section, we investigate the mechanisms of slow-earthquake migration by comparing observational results and numerical simulation results. One of possible mechanism is chain reaction of numerous small asperities (Fig. 1), which is based on the activity of small

repeating earthquakes triggered by afterslip of large interplate earthquakes (Matsuzawa et al., 2004).

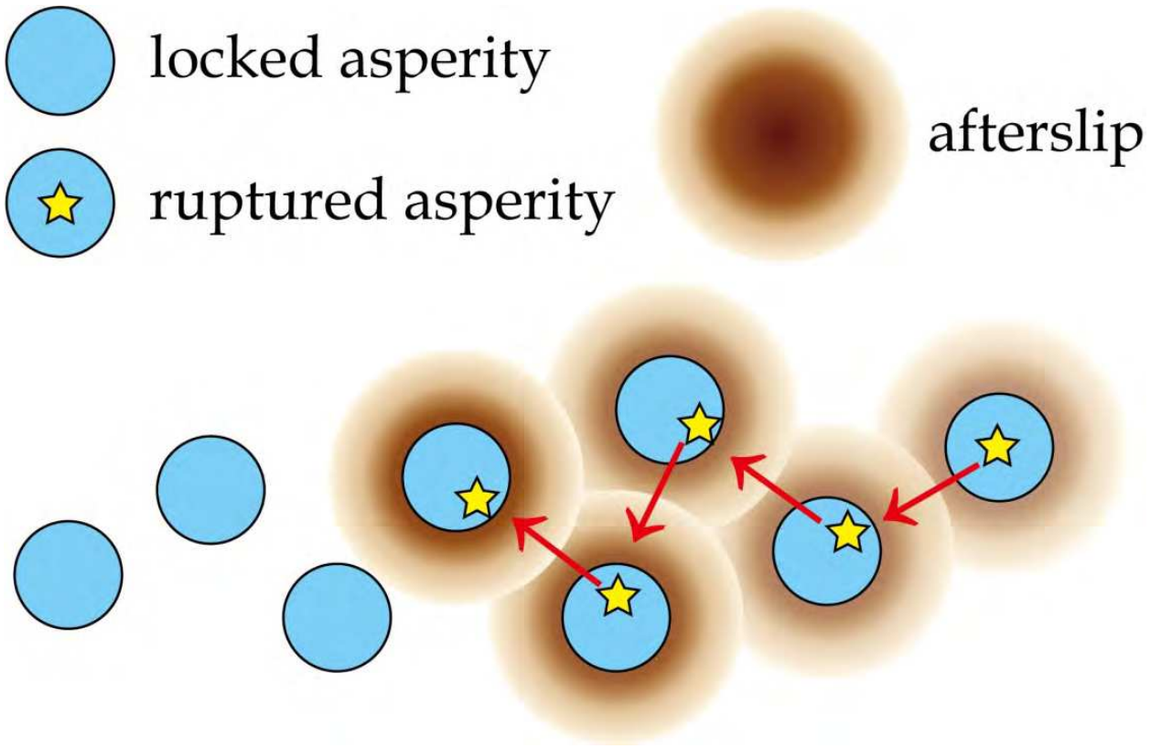

Fig. 1. A schematic model of chain-reaction between asperities after Matsuzawa et al. (2004). Yellow stars represent rupture initiation points of slip events.

On the other hand, some simulation results show slow-earthquake migration is reproduced by models with frictional properties almost uniform along strike and constant effective normal stress independent of depth under initial stress uniform along strike (e.g., Liu & Rice, 2005). Their simulation results suggest that an essential condition for the slow-earthquake migration is neither heterogeneous frictional properties nor heterogeneous initial stress distribution, if effective normal stress is constant at low value and independent of depth.

In the case of effective normal stress proportional to depth for a model with uniform frictional properties, slow-earthquake migration does not occur (e.g., Hirose & Hirahara, 2002). Note that above all simulation studies adopt the same friction law. These previous simulation results raised the following question: For an asperity model with low effective normal stress around 30 km depth, are small asperities essential for the slow-earthquake migration?

In this section, we formulate several test models in order to understand the necessary conditions and characteristics for slow-earthquake migration.

2.1 A test model of chain reaction between numerous small asperities

A test model consists of a planar plate interface dipping at 15 degrees from the free surface in a homogeneous elastic half-space (Fig. 2) with a periodic boundary condition along the strike direction. The plate interface is divided into 1,024 (strike) × 293 (dip) cells.

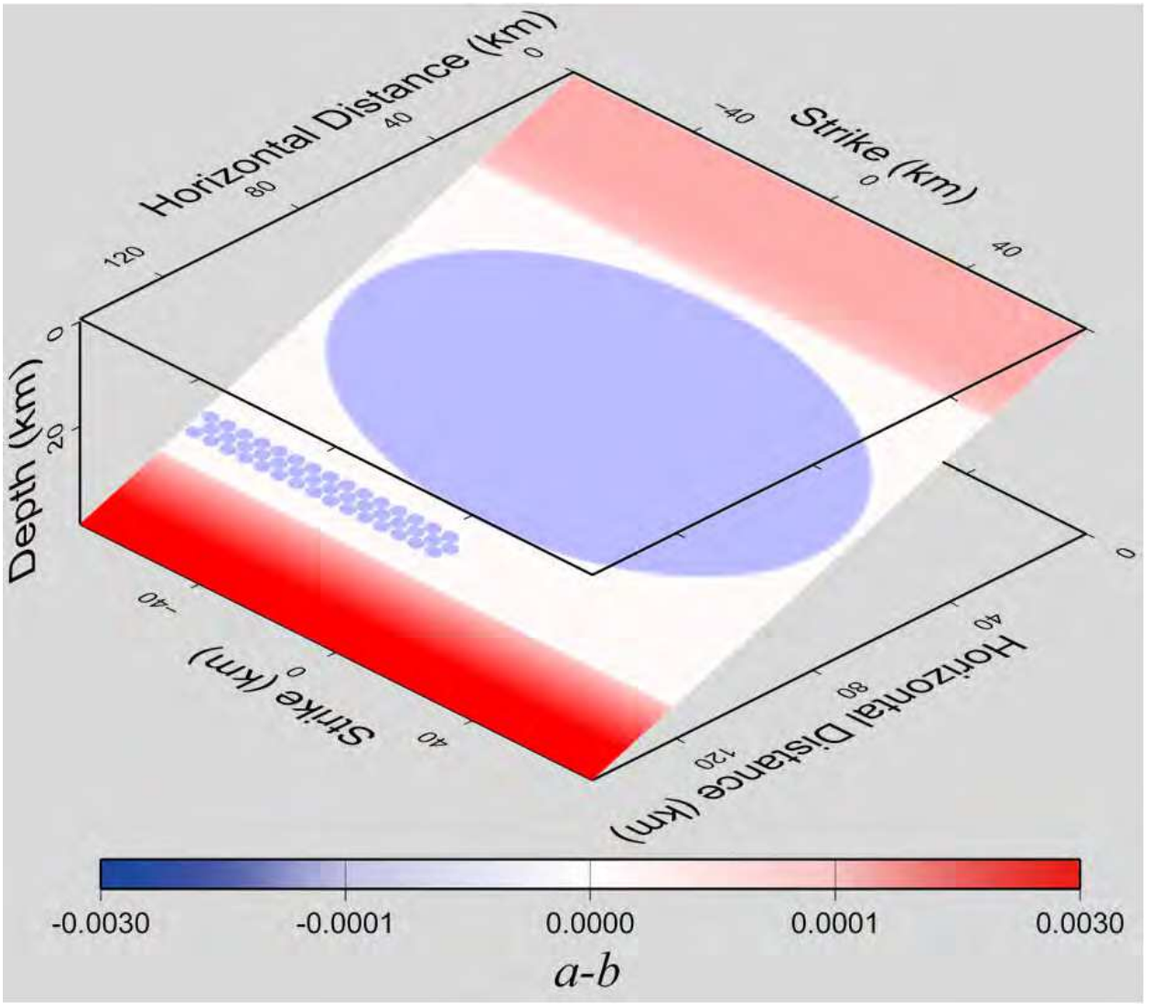

Fig. 2. A 3-Dimensional model of a subduction plate boundary with frictional parameter *a-b* (Eq. 3). Cool color represents asperity.

Slip is assumed to occur in the pure dip direction and to obey the quasi-static equilibrium between shear and frictional stresses by introducing a radiation damping term (Rice, 1993):

$$\mu_i \sigma_i = \sum_{j=1}^{N} K_{ij}(u_j(t) - V_{\mathrm{pl}}t) - \frac{G}{2\beta}\frac{\mathrm{d}u_i}{\mathrm{d}t} \tag{1}$$

Here, the subscripts i and j denote the location indices of a receiver and a source cell, respectively. The left hand side of equation (1) describes frictional stress, where μ and σ is friction coefficient and effective normal stress, respectively. The right hand side describes the shear stress in the i-th cell caused by dislocations, where K_{ij} is the Green's function for the shear stress (Okada, 1992) on the i-th cell, N is the total number of cells, V_{pl} is the relative speed of the two plates, t denotes time, G is rigidity, β is the shear wave speed. K_{ij} is calculated from the quasi-static solution for uniform pure dip-slip u relative to average slip $V_{\mathrm{pl}}t$ (Savage, 1983) over a rectangular dislocation in the j-th cell. Parts of the first term of the right-hand side are written as convolutions, by exploiting the along-strike invariance of the

Green's function, and efficiently computed by the Fast Fourier Transform (e.g., Rice, 1993; Liu & Rice, 2005).
In Eq. (1), the effective normal stress σ is given by

$$\sigma_i(z) = \kappa(z)(\rho_{\mathrm{rock}} - \rho_{\mathrm{w}})gz, \tag{2}$$

where ρ_{rock} and ρ_{w} are the densities of rock and water, respectively, g is the acceleration due to gravity, and z is the depth. The function $\kappa(z)$ is a super-hydrostatic pore pressure factor, as given in Fig. 3. We assume that a high-pore-pressure system locally exists around a depth of 30 km based on the high-$V_{\mathrm{p}}/V_{\mathrm{s}}$ zones in southwestern Japan (e.g., Shelly et al., 2006). The increase in pore pressure is probably due to the dehydration derived from the change in facies in the slab (e.g., Hacker et al., 2003). Ariyoshi et al. (2007) estimated that the value of κ is 0.1 for the deeper part (>30 km depth) based on the post-seismic slip propagation speed. On the basis of the stress field observation in northeastern and southwestern Honshu, Japan, Wang & Suyehiro (1999) suggested that the apparent frictional coefficient is approximately 0.03, which is consistent with $\kappa = 0.1$.
The friction coefficient μ is assumed to obey an RSF law (Dieterich, 1979; Ruina, 1983), as given by

$$\mu = \mu_0 + a \log (V/V_0) + b \log (V_0\theta/d_{\mathrm{c}}), \tag{3}$$

$$\mathrm{d}\theta/\mathrm{d}t = 1 - V\theta/d_{\mathrm{c}}, \tag{4}$$

where a and b are friction coefficient parameters, d_c is the characteristic slip distance associated with b, θ is a state variable for the plate interface, V is the slip velocity, and μ_0 is a reference friction coefficient defined at a constant reference slip velocity of V_0.
We consider a model with close-set numerous small asperities on the deeper outskirt of a great asperity, as proposed by Dragert et al. (2007). In the present study, an asperity denotes a region with a-$b = \gamma < 0$, following Boatwright & Cocco (1996). The plate interface is demarcated into five parts, as shown in Figs. 2 and 3: (i) one large asperity (LA), (ii) 90 small asperities (SAs), (iii) a shallow stable zone, (iv) a deep stable zone, and (v) a transition zone ($\gamma \sim +0$). The values of frictional parameters as described in the caption of Fig. 3 are based on rock laboratory results (e.g., Blanpied et al., 1998), which will be discussed later.
The constant parameters in the present study are $V_{\mathrm{pl}} = 4.0\times10^{-2}$ m/yr (or 1.3×10^{-9} m/s), $G = 30$ GPa, $\beta = 3.75$ km/s, $\rho_{\mathrm{rock}} = 2.75\times10^{3}$ kg/m^3, $\rho_{\mathrm{w}} = 1.0\times10^{3}$ kg/m^3, $g = 9.8$ m/s^2, $V_0 = 1$ μm/s, $\mu_0 = 0.6$, and Poisson's ratio $\varepsilon = 0.25$.

2.2 Simulation results of chain reaction effect on low-frequency event migration

Fig. 4 shows the spatial distribution of slip velocity about 37 years before the origin time of a megathrust earthquake in the large asperity. The recurrence interval and magnitude of the megathrust earthquake in our simulation is 116 years and M_{w} 7.9, respectively, where seismic slip is defined as slip faster than 1 cm/sec. The large asperity (LA) is strongly locked while a slow-earthquake occurs in some of small asperities (SA).
Fig. 5 shows time history of velocity field before and after the megathrust earthquake. Figures 2 and 3 suggest slow-earthquake migration at the migration rate of 0.3~3 km/day, which is driven by the chain reaction of small asperities. On the other hand, these figures also show that slow-earthquake migration does not usually occur in the region without small asperities, where slip velocity is largely stable at values comparable to V_{pl}.

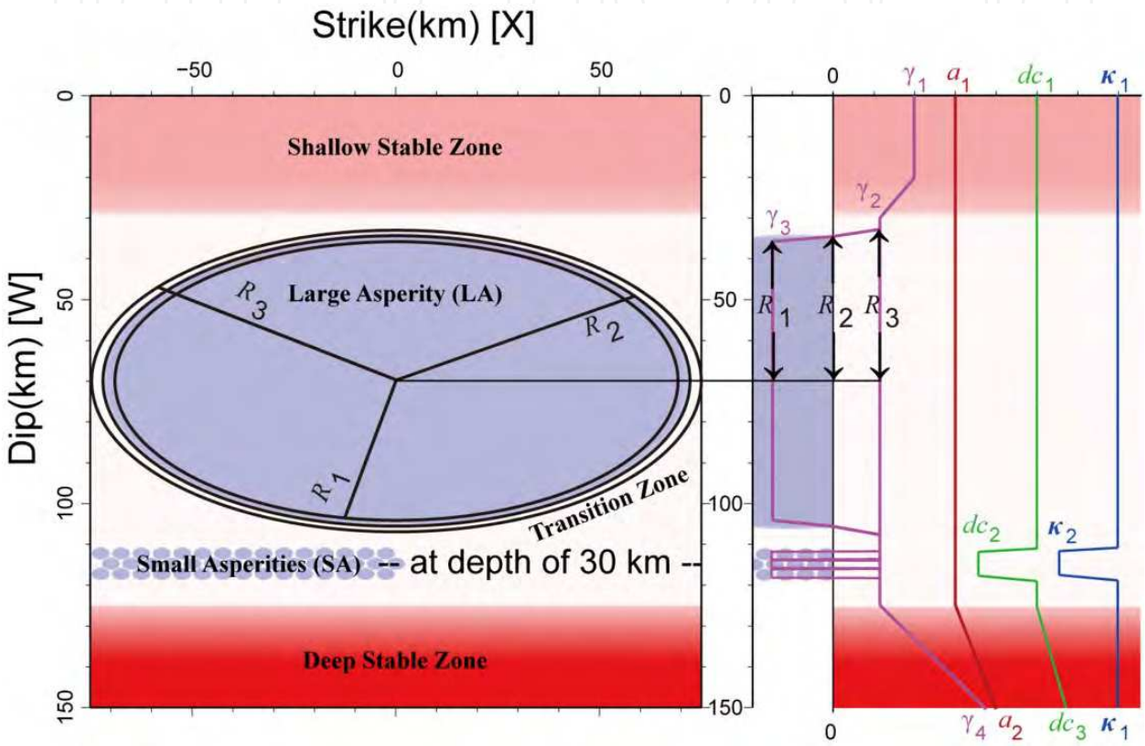

Fig. 3. Frictional parameters (a, γ (= a-b), d_c, κ (See Eq. (2)) as functions of distance along the dip direction from the surface on the plate boundary, where (a_1, a_2) = (2, 5) [×10^{-3}], (γ_1, γ_2, γ_3, γ_4) = (0.5, 0.01, -0.3, 4.9) [×10^{-3}], (d_{c1}, d_{c2}, d_{c3}) = (10, 0.43, 100) [mm], and (κ_1, κ_2) = (1.0, 0.1). Half the length of the minor axis (along dip) of the elliptical asperity takes the following values: for LA, (R_1, R_2, R_3) = (35, 36.25, 37.5) [km] and for SA, (r_1, r_2, r_3) = (1.33, 1.5, 1.67) [km], where the aspect ratios for LA and SA are 2.0 and 1.5, respectively. The distance between central points of SA along strike and dip direction is 2 and 2.5 km, respectively. This figure is developed from Ariyoshi et al. (2011a).

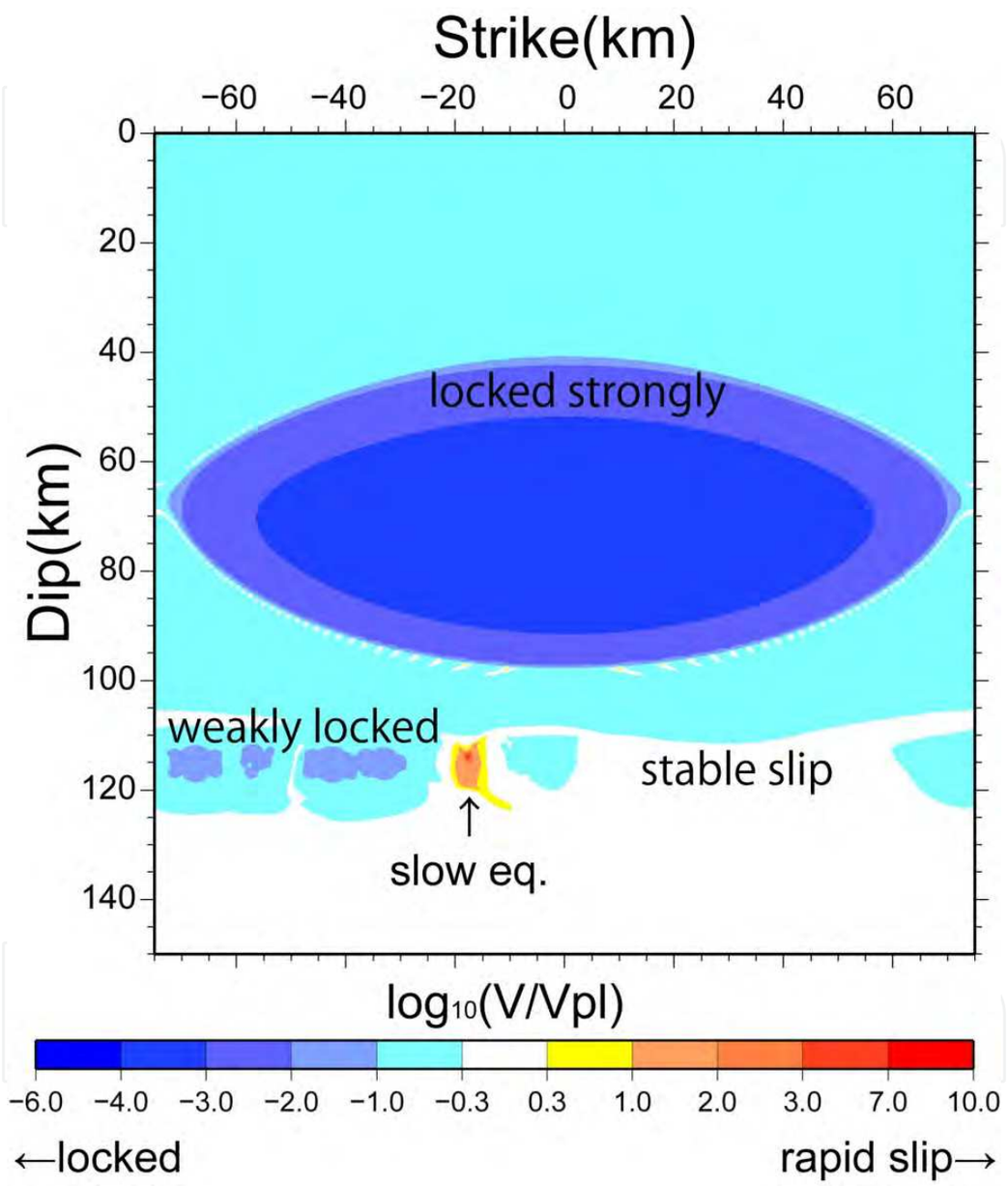

Fig. 4. Velocity field on the subduction plate boundary 36.6 years before the megathrust earthquake. Note that 8 of $\log_{10}(V/V_{\mathrm{pl}})$ is about 1 cm/sec. This figure is developed from Ariyoshi et al. (2011a).

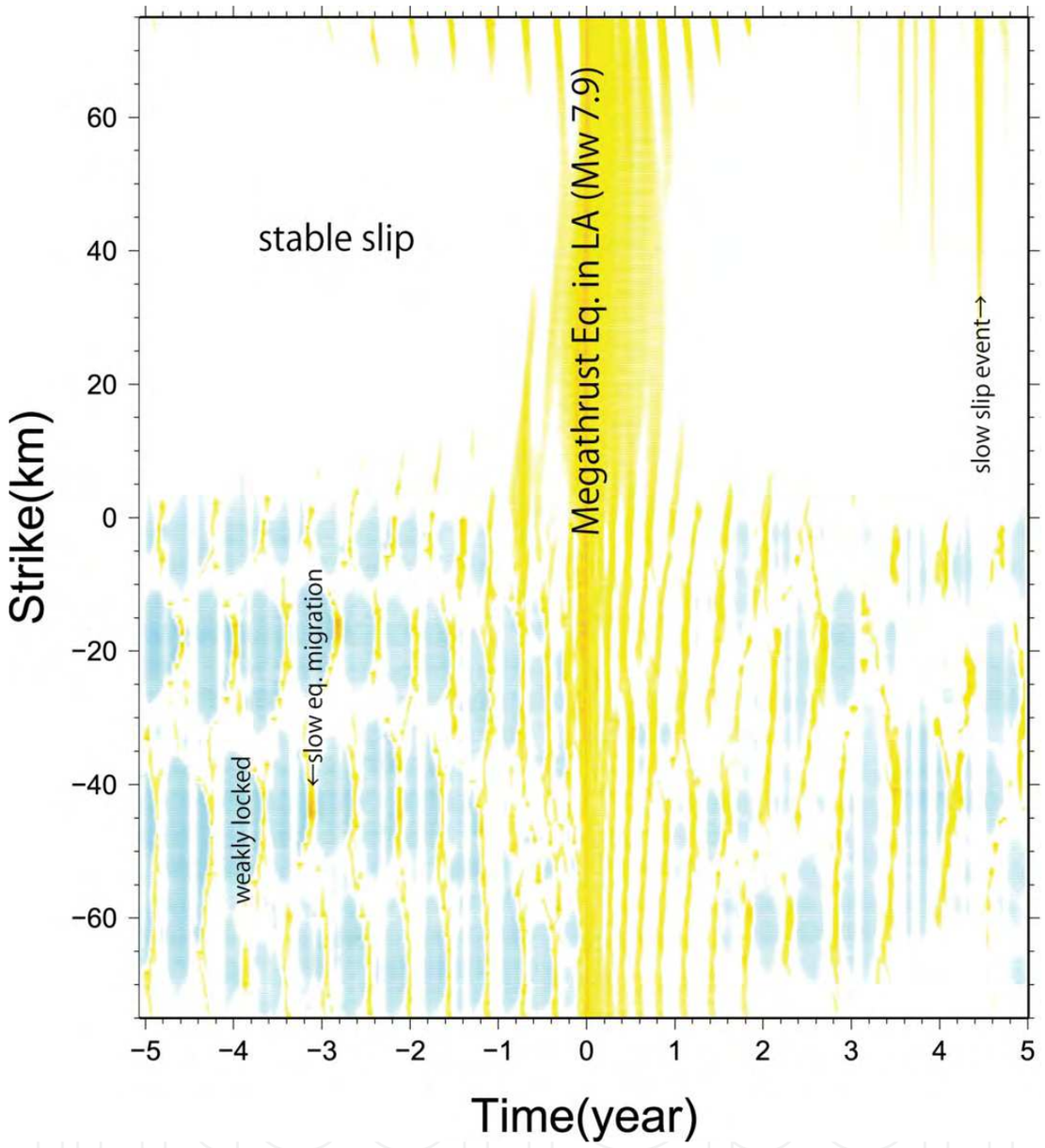

Fig. 5. Spatiotemporal evolution of slip velocities at the "Dip" of 115 km along strike as shown in Fig. 3 before and after the megathrust earthquake in case that numerous small asperities in Fig. 3 are removed for Strike>0. Color scale is the same as Fig. 4. This figure is developed from Ariyoshi et al. (2011a).

After about 4.5 years after the megathrust earthquake in Fig. 5, the largest slow slip event (~ 10 V_{pl} at most; much slower than slow-earthquakes in Fig. 5) occurs in the region without small asperities. Since all of slow slip events in the region without small asperities originate from the transition between SA-belt and no-SA (between Strike = 0 and 75 km due to the cyclic boundary condition along strike direction), these slow slip events are triggered by the chain reaction of SA.

2.3 Size effect of small asperities on chain reaction behaviors

Next, we perform another test model with different size of asperity generating chain reaction as shown in Fig. 6 in order to investigate size effect.

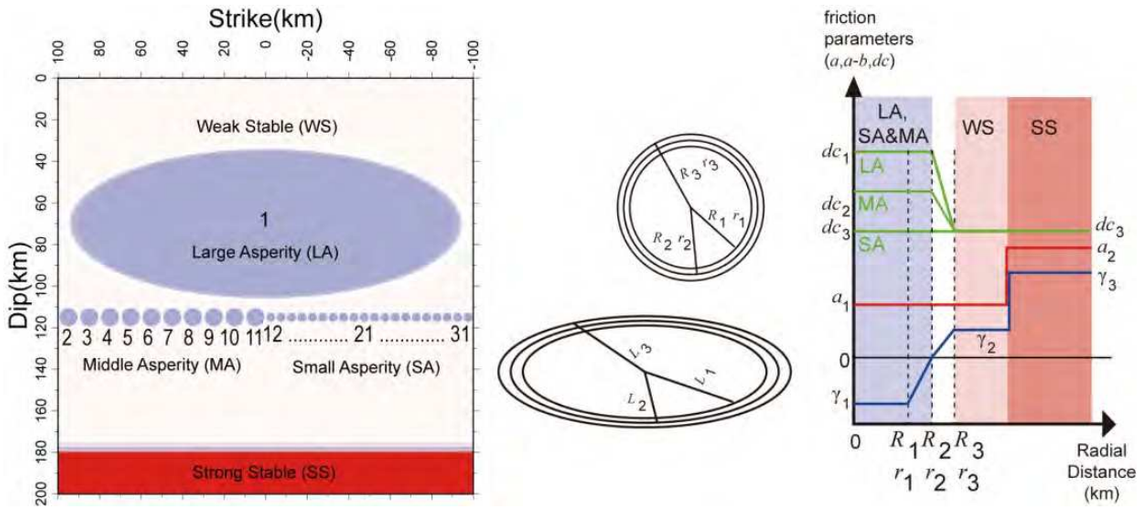

Fig. 6. Spatial distribution of large asperity (LA), middle asperity (MA), small asperity (SA) (a-b < 0) with identification numbers of the asperities, weak stable (WS; a-$b \geq 0$) and strong stable (SS; a-b >> 0). Setting fault geometry, elevated pore pressure, and the constant value of other geophysical parameter is the same as section 2.2. This figure is partly derived from Ariyoshi et al. (2009).

Figs. 7a-7k shows simulation results of slip migration driven by chain reaction of asperities. For MA (left panel of Figs. 7a-7e), unilateral chained propagation process is clearly seen for MA, with propagation speed between asperities No. 7 to No. 5 of about 0.2 km/day (Figs. 7b-d). In the time span indicated by the cyan background in Figs. 7l-m, the patterns of stress drop and averaged slip velocity at asperities No. 3 to 5 appear to be relatively similar but quantitatively different. Especially, the amount of stress drop and averaged slip velocity in asperity No. 3 is greater than in the others. In addition, there is not only leftward chained propagation from the asperity No. 10 but also rightward propagation from the asperity No. 2, where the latter is much slower than the former because of the large area locked in the asperity No. 3. In Fig. 7e, both chained propagations cross at the asperity No. 3, which promotes larger stress drop and higher slip velocity. Since similar behavior seems to be seen in the simulation of Liu & Rice (2005), these results suggests that some phenomena generated by introducing along-strike variations of constitutive parameters or non-uniform initial conditions may be represented by interaction between small asperities.

On the other hand, the propagation process of SA is different from that of MA in some respects. On the right side of Fig. 7 shows leftward propagation from the asperity No. 2 through No. 31 to No. 22, which is due to the periodic boundary condition. In the time span indicated by a green background in Figs. 7n-o, there are two slow earthquakes for each asperity from No. 28 to 31. Propagation speed between asperities No. 31 to 28, No. 28 to 23 and No. 23 to 22 is about 0.2, 0.15 and 0.03 km/day, respectively, which progressively becomes slower than that of MA. Fig. 7j shows that rightward propagation from the asperity No. 27 and 30 is also seen.

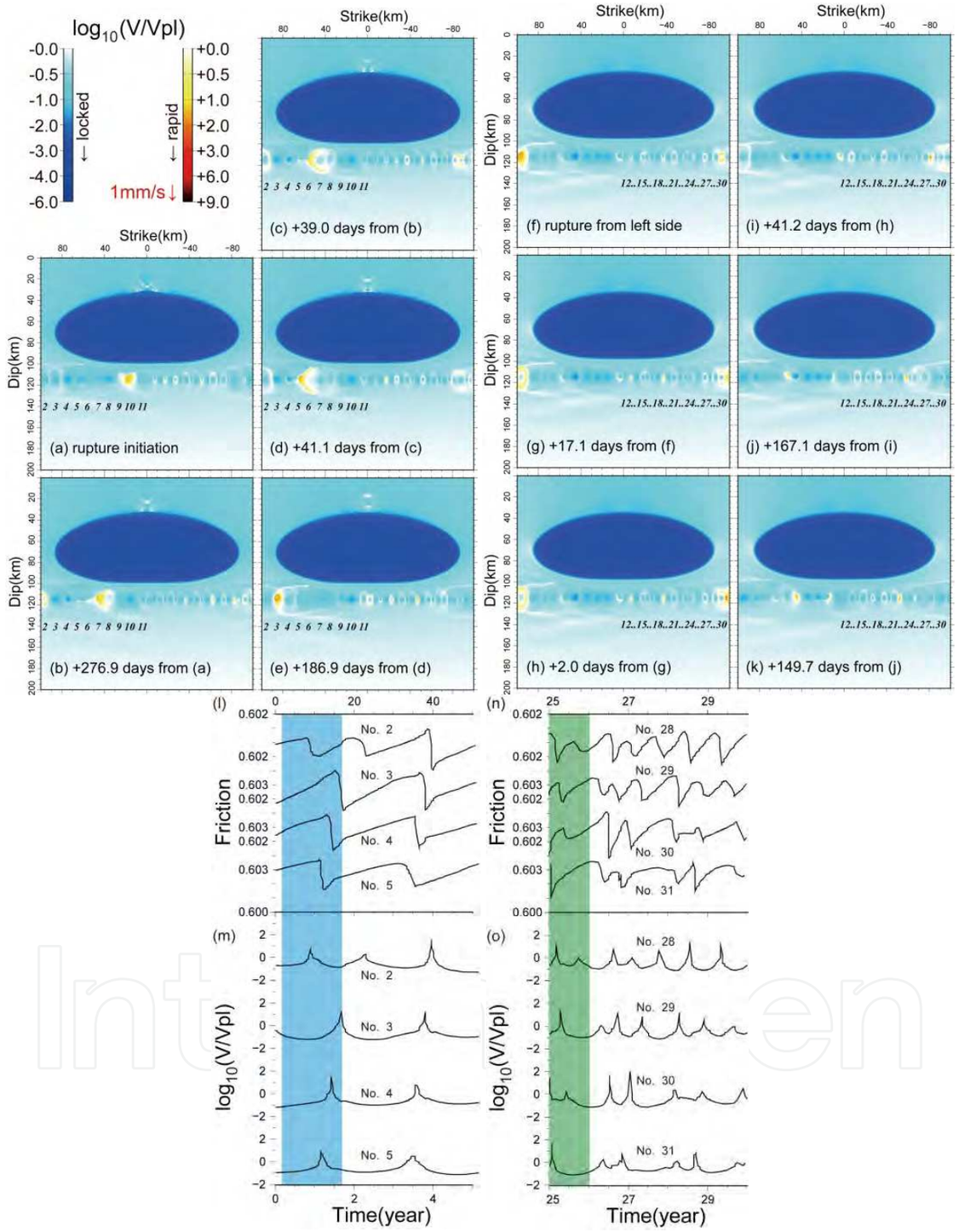

Fig. 7. Examples of chain-reaction between asperities for MA (left panels (a)-(e)) and SA (right panels (f)-(k)) with time history of friction and normalized slip velocity averaged in each asperity (MA; (l)(m), SA; (n)(o)) after Ariyoshi et al. (2009). Italic numbers are identification of asperities. Cyan and green regions correspond to time spans of snapshots for MA and SA, respectively.

These differences from MA are explained as follows. SA has shorter recurrence intervals and smaller moment release because of smaller asperity size with shorter characteristic distance than those of MA. The smaller moment release makes propagation speed slower (0.03 km/day for SA is smaller than 0.2 km/day for LA), which causes that recurrence interval of SA is relatively much shorter than the passage time of aseismic slip across more than twice the SA diameters (10 km). In addition, locking of SA soon after the occurrence of slow earthquakes, due to their short characteristic distance, tends to prevent aseismic slip propagation. Therefore, slow earthquakes occur again soon after the passage of aseismic slip from asperity No. 29 as shown in Figs. 7n-o. This is why propagation process of SA as shown in Figs. 7n-o appears to be bilateral, rather than the unilateral propagation seen in Figs. 7a-7e.

2.4 Discussions of chain reaction effect on slow earthquake migration

Fig. 5 clearly shows that only slow slip events occur at depth of 30 km where frictional property is slightly stable and uniform along strike, while various slow earthquakes including very low-frequency events (orange color in Fig. 5) are generated by chain reaction between small asperities. This result suggests that chain reaction model as shown in Fig. 1 can explain various types of slow earthquakes occur in the same region.

Fig. 7 shows that MA has recurrence interval longer than that of SA, which is also seen for migration distance. These results may suggest that we can estimate asperity size on the basis of migration distance and recurrence interval of slow earthquakes.

For example, migration of low-frequency tremor observed in Kii and Tokai area tends to be unilateral with longer travel distance and loger recurrence interval of slip events, while the tremor in Shikoku tends to be shorter recurrence interval and shorter travel distance (e.g., Obara, 2010). These results suggest that size of asperities generating slow earthquakes in Kii and Tokai is larger than that in Shikoku. Therefore, investigating slow earthquake migration process is important to estimate the characteristics of small asperities.

3. Application to the detection of preseismic slip for megathrust earthquakes

As pre- and post-seismic changes, intense LFT activity began to occur almost directly below the 2004 Parkfield earthquake about three weeks before the earthquake and has continued only apart from the hypocenter over for four years (Nadeau & Guilhem, 2009; Shelly, 2009), which means that the distance from the hypocenter of triggering earthquake may also affect the sensitivity of LFT to pre- and post-seismic slip (Shelly, 2009).

In this section, we try to apply preseismic change of slow earthquake migration to the detection of megathrust earthquakes on the basis of characteristics of slow earthquake migration as described in the section 2.

3.1 A test model of slow earthquake migration for long travel distance

Fig. 8 shows a 3-D model of a subduction plate boundary derived from Fig. 2. Its frictional parameter is the same as Fig. 3 in order to investigate slow earthquake migration for long distance across the center of large asperity along strike direction as observed south-western Japan (Obara, 2010).

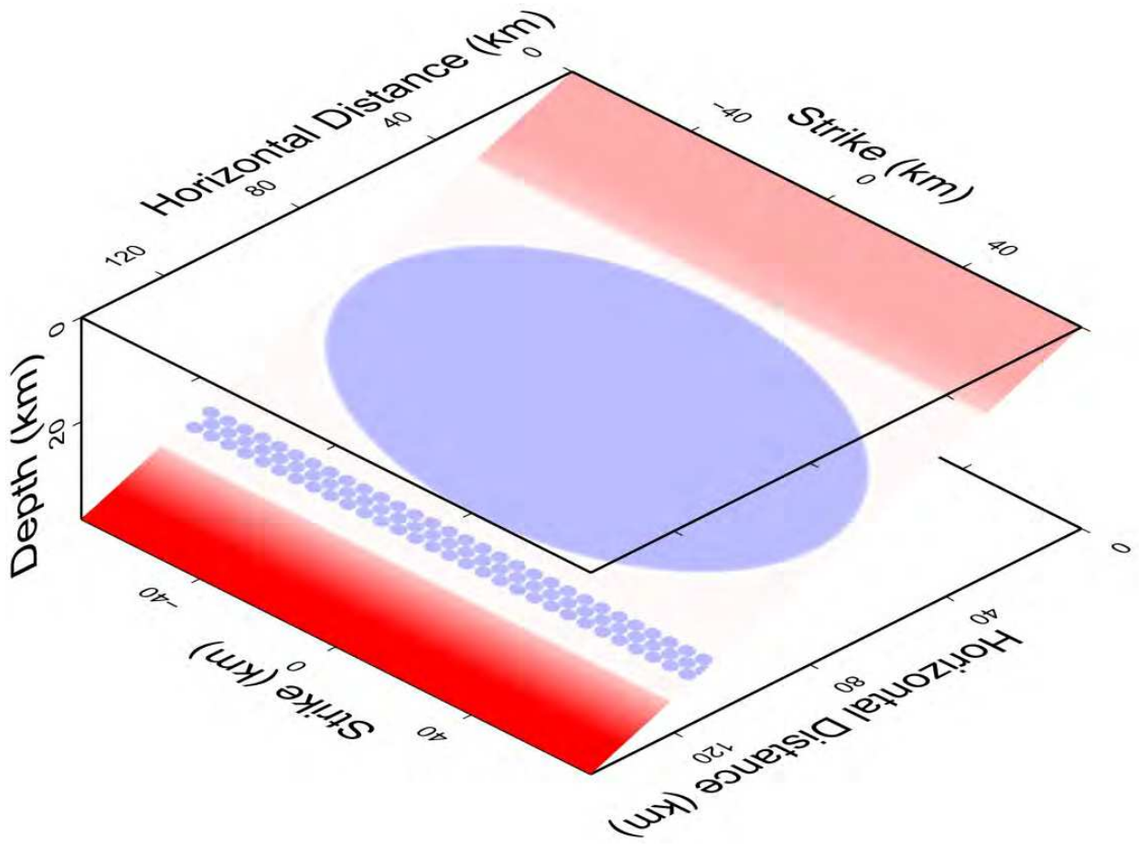

Fig. 8. A 3-Dimensional model of a subduction plate boundary with frictional parameter a-b (Eq. 3), where the color scale is the same as Fig. 2.

3.2 Long-term change in the migration speed of slow earthquake swarms

Figs. 9a and 9b show the spatiotemporal evolution of the slip velocity normalized by V_{pl} at 115 km down-dip from the trench (along green line in Figs. 9d and 9e) in the interseismic and preseismic stages, respectively. Close-up of the slip velocity pattern in the rectangle in Fig. 9b is shown in Fig. 9c. Figs. 9d and 9e show the snapshots of the normalized slip velocity 20 years after and 0.86 years before a megathrust earthquake, respectively.

Based on Figs. 9a-9c, we calculate the migration speeds of slow earthquake swarms by tracking transients with slip rate ranging from 2 to 10 V_{pl} (indicated by yellow color). Periods of larger slip rate (from 10 to 100 V_{pl} indicated by orange colors) are difficult to find in Fig. 9b because of their short duration, except for times later than -0.2 years in Fig. 9b.

The dominant migration speed is calculated to be approximately 0.3 to 1 km/day during the interseismic stage (Fig. 9a), while 1 to 3 km/day in the preseismic stage (Fig 9b). Therefore, the simulation results suggest that monitoring of the migration speeds of slow earthquake swarms as well as recurrence intervals are useful to forecast great earthquakes.

Approximately one month before the megathrust earthquake, Fig. 9b shows that the dominant slip velocity for $|\mathrm{Strike}| < 40$ km becomes higher than 10 V_{pl} (orange) and is sustained over a long duration time (more than one month). This implies that the moment release rates of slow earthquake swarms near the locked region of LA just before a megathrust earthquake tend to be significantly higher than that in the interseismic stage.

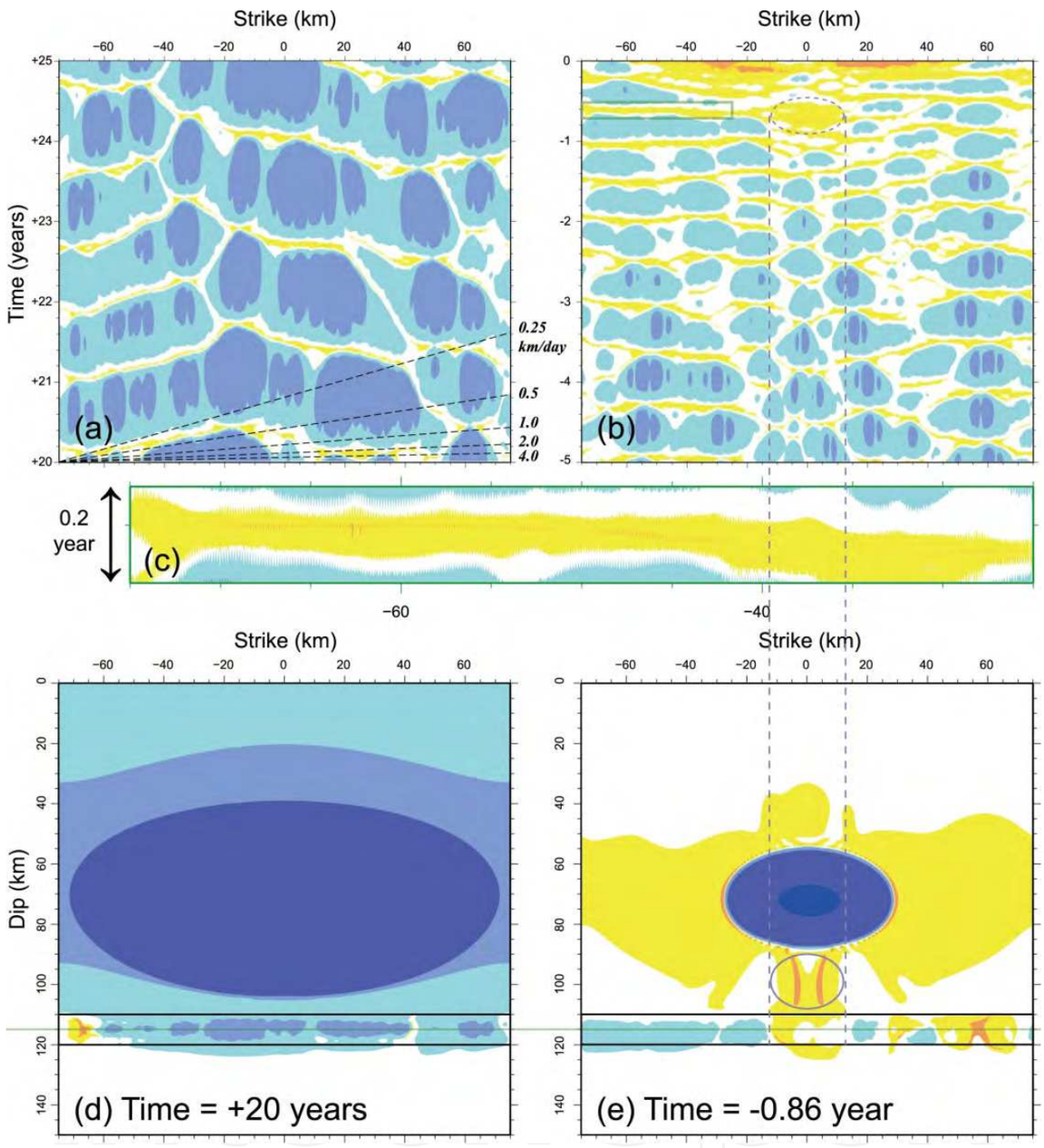

Fig. 9. (a)(b) Spatiotemporal evolution of slip velocities at the "Dip" of 115 km along strike (green line in Figs. 9d and 9e) in the interseismic and preseismic stages, respectively, after Ariyoshi et al. (2011b). Color scale is the same as Fig. 4. The broken lines in (a) denote the migration speed in km/day. (c) Close up of the slip velocity evolution in the spatiotemporal region enclosed by the green rectangle in (b), keeping the aspect ratio of space to time. (d)(e) Snapshots of the slip velocity field (d) 20 years after and (e) 0.86 year before the occurrence time of the megathrust earthquake. The ellipse enclosed by the purple curve in (e) represents a large aseismic slip event activating slow earthquakes as shown by the ellipse in (b).

Fig. 9d suggests that the slip velocity is approximately less than 0.5 V_{pl} (aqua) in the region surrounding the SA (boxed area) and less than 0.1 V_{pl} (blue) dominantly along the center of

the SA belt (green line), except for the region where a slow earthquake migration occurs (yellow and orange). Fig. 9e suggests that the area of higher slip velocity (orange) covering SAs in the preseismic stage tends to be larger than in the interseismic stage as shown in Fig. 9d, and there is no region in which the slip velocity is less than 0.1 V_{pl}. Slip velocity in LA becomes higher due to the preseismic slip, especially about one year before the megathrust earthquake. These results mean that preseismic slip of LA promotes higher moment release rates of slow earthquake due to its higher slip velocity.

3.3 Comparison of slow earthquakes between simulation and observational results

Fig. 9e shows that a large aseismic slip event occurs locally between LA and the SA belt (indicated by the ellipse) approximately one year before the megathrust earthquake. The spatiotemporal region enclosed by the ellipse in Fig. 9b shows that the large aseismic slip event triggers slow earthquakes in the SA belt with a shorter recurrence interval compared to other areas (|Strike| > 20 km). The migration distance in the SA belt corresponds to the size of the large aseismic slip region (|Strike| < 20 km). This behavior is similar to the long-term SSE (slow slip event) observed at Bungo Channel in 2003, where nearby LFT (low frequency tremor) migration had occurred either at a shorter recurrence interval or nearly continuously for several months (Obara, 2010). Therefore, the activity of the LFTs may be useful to estimate the duration and the location of local aseismic slip events, such as the long-term SSE and the preseismic slip in the deeper part of LA.

As pre- and post-seismic changes, intense LFT activity began to occur almost directly below the 2004 Parkfield earthquake about three weeks before the earthquake and has continued only apart from the hypocenter over for four years (Nadeau & Guilhem, 2009; Shelly, 2009), which means that the distance from the hypocenter of triggering earthquake may also affect the sensitivity of LFT to pre- and post-seismic slip (Shelly, 2009).

Our simulation shows that the moment release rate of slow earthquakes near the locked region of LA becomes higher about one month before the megathrust earthquake as mentioned in the section 3.2, and Figs. 9ab show that a shorter recurrence interval of slow earthquakes in the SA belt occurs several years after the megathrust earthquake. These simulation results are consistent with those results observed in Parkfield for the pre- and post-seismic stages of nearby large earthquakes.

Since SSE, pre- and post-seismic slips are all transients of interplate-slip faster than V_{pl}, the observations reported by Obara (2010), Nadeau & Guilhem (2009), and Shelly (2009) would support our suggestion that the preseismic slip of megathrust earthquakes can be practically detected by monitoring slow earthquake migrations, even if the actual d_c is less than several centimeters.

4. Monitoring slow earthquakes in shallower part by DONET

Recently, slow earthquakes have been also observed in shallower part of subduction plate boundaries (e.g., Hirose et al., 2010). As seen in Figs. 9d and 9e, stress shadow of LA has more effective on shallower part of transition zone. This means that preseismic change of slow earthquake may be more sensitive in the shallower part. In this section, we develop a model of slow earthquake migration in shallower part of transition zone in addition to deeper part, discussing the detectablity of Dense Oceanfloor Network System for Earthquakes and Tsunamis (DONET) toward an anticipated Tonankai Earthquake (Fig. 10).

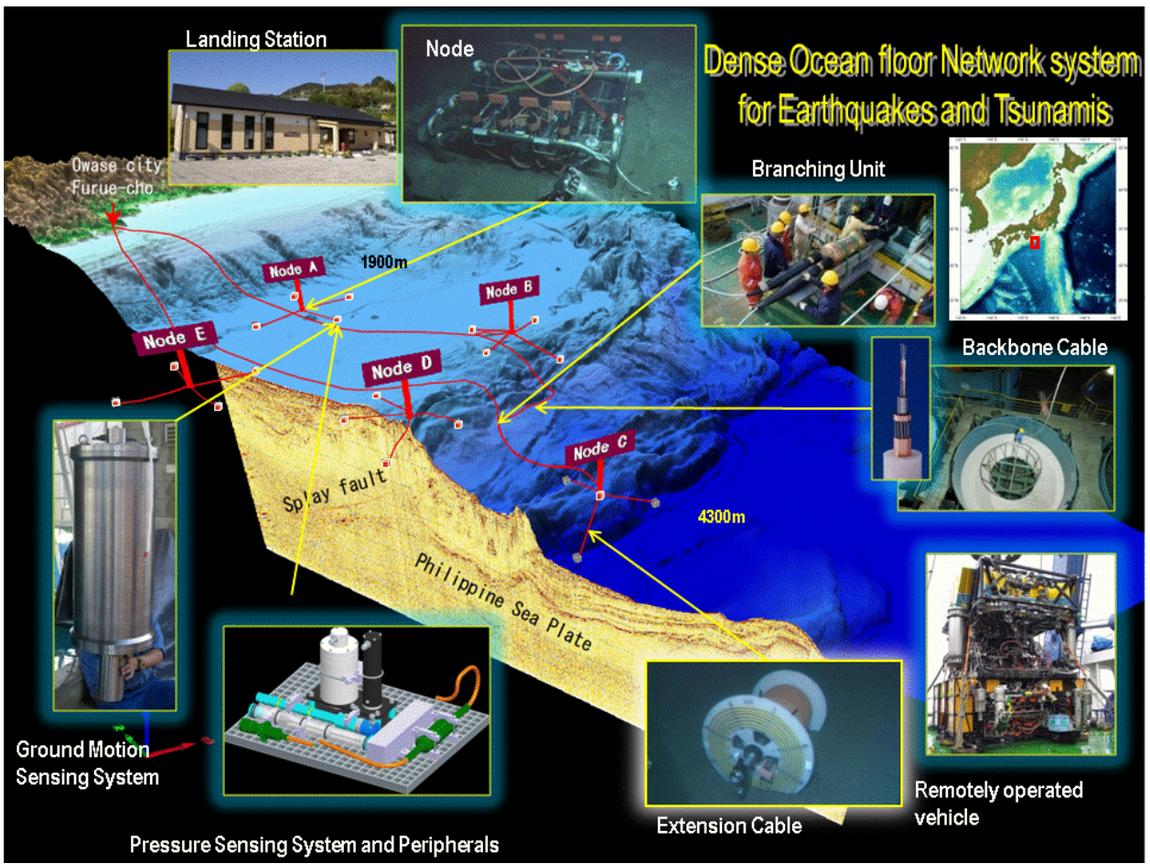

Fig. 10. An overview of Dense Oceanfloor Network System for Earthquakes and Tsunamis (DONET) in Tonankai region.

4.1 Design concept of DONET toward forecasting the Tonankai earthquake

In Fig. 10, DONET has a submarine cabled real-time seafloor observatory network for the precise earthquake and tsunami monitoring. For the purpose of understanding and forecasting the earthquake and related activities underneath the seafloor, the twenty sets of state-of-arts submarine cabled sub-sea measurement instrument will be deployed in seafloor at the interval of 15-20km. All of the twenty sets of preliminary interface have been installed just on July 31, 2011 and are to be prepared in consideration of the improvement of observation capability in the future.

As described by Kawaguchi et al. (2011), operating large-scale subsea infrastructure over a long period of time (20-30 years) is one of a challenge of underwater technology. The increase of measurement instruments has a big influence on the total system reliability, because of the state-of-arts instrument is a bottleneck to maintain long-term reliability. A novel system design concept is necessary for the observatory network development to make two demands such as 'high reliability system design' and 'state-of-arts measurement' united. The observatory network should be able to replace, maintenance and extend while operating, and should be have a redundancy for the internal or external observatory network component failure. To achieve these requirements, DONET adapt a strategy to combining the following three major components with different system reliability: (i) high

reliability backbone cable system, (ii) replaceable science node, and (iii) extendable measurement instruments.

4.2 Expectation of preseismic monitoring by DONET

Fig. 11 shows a map projection of 3-D subduction plate boundary model in Tonankai region. In this study, we introduce a plate interface bended by spline curve along dip direction, taking it into account the structural survey published by Nakanishi et al. (2008). hypocenter of shallower part of slow earthquakes is mainly based on the recent studies (e.g., Obara & Shiomi, 2009).

Megathrust earthquake (M_w 8.2) occurring in LA has periodic recurrence time of 113 years. Fig. 12 shows snapshot of slip velocity field in the interseismic and preseismic stage of the megathrust earthquake. Comparing shallower part of slow earthquake activity with deeper part, we found that the shallower part of slow earthquakes is less active than the deeper part in the interseismic stage of the megathrust earthquake (in the top of Fig. 12), because stress shadow from LA has more effective on the shallower part. In the preseismic stage (in the bottom of Fig. 12), the shallower part of slow earthquake comes to be similar to the deeper part and to be more active especially around the center of LA, because locked region is only around the center of LA and slip deficit in the preseismic stage is more than deeper part. These simulation results suggest that monitoring the shallower part of slow earthquakes may be effective on the ground that it is more sensitive to the preseismic change of the megathrust earthquake because of free surface condition.

In order to detect the preseismic slip of the next Tonankai earthquake in the near future, DONET would play an important role in monitoring shallower part of slow earthquake migration from the view of shortening recurrence interval and increasing migration speed as pointed out in the section of 3.2. Considering the location of 20 observation points as shown in Fig. 11 and numerical simulation results in Figs. 11 and 12, we expect DONET to do precise detection of preseismic change of the Tonankai earthquake as listed in Table 1.

	Long	Short	Coverage	Dislocation	Main	Afterslip
Node A	○	◎		○	◎	
Node B	○	◎	◎	◎		
Node C	○	○	◎	◎		○
Node D	◎	○	◎	◎		○
Node E	◎	○		○	◎	

Table 1. DONET's major roles in monitoring seismic & crustal change due to the Tonankai earthquake.

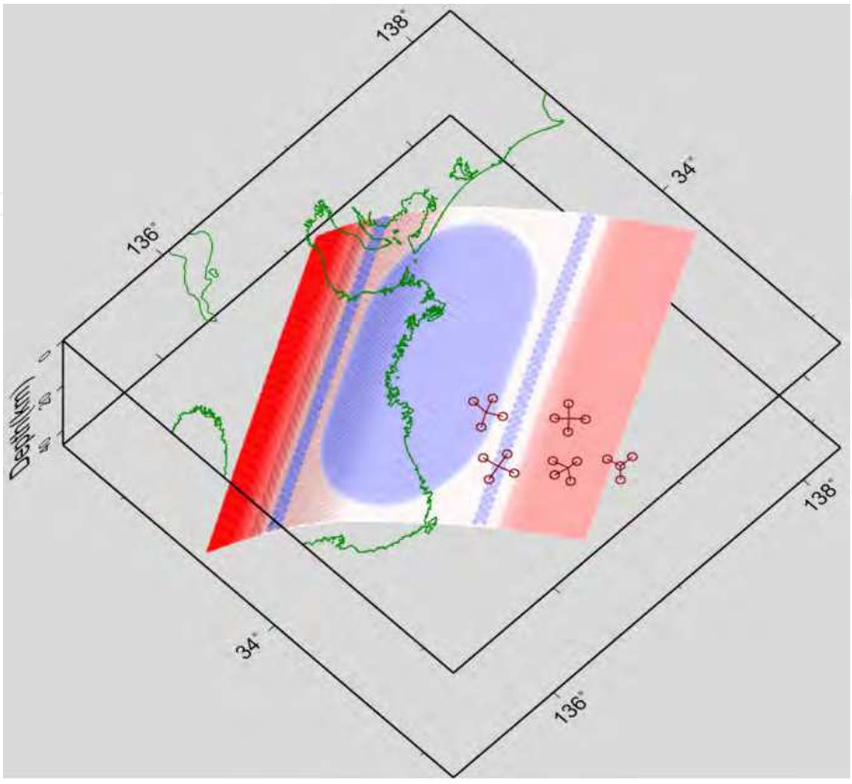

Fig. 11. A 3-D map projection of a subduction plate boundary model for Tonankai earthquake. Frictional parameter for Shallow Stable Zone, Deep Stable Zone, Large & Small Asperity, and Transition Zone is the same as Fig. 3 but (κ_1, κ_2) = (0.3, 0.1) on the basis of afterslip propagation speed investigated by Ariyoshi et al. (2007) and the value of d_{c2} for SA in shallower part is 0.3 mm. Note that we use shade effect on the color scale by applying the command "grdgradient" (Wessel & Smith, 1998) in order to show the bending shape visually. Twenty open circles with five nodes represent observation points of DONET as shown in Fig. 10.

"Long" & "Short" represent long-term & short-term forecast based on recurrence interval and migration speed of slow earthquakes, respectively. "Coverage" represents significant effect on estimating hypocenters of slow earthquakes with high precision due to the coverage from trench side. "Dislocation" represents key observation points for estimating slip amount of continental plate relative to oceanic plate. "Main" represents main part of seismic slip process generated from LA. "Afterslip" represents aseismic slip along trench which may triggers nearby Nankai earthquake.

On the basis of numerical simulation results as shown in Fig. 12 and Table 1, DONET is expected to play important role in monitoring preseismic change of the next Tonankai earthquake from the view of various points including shallower part of slow earthquake activity and in judging the possibility of triggering the nearby Nankai earthquake, which had occurred in 1946 two years after the 1944 Tonankai earthquake.

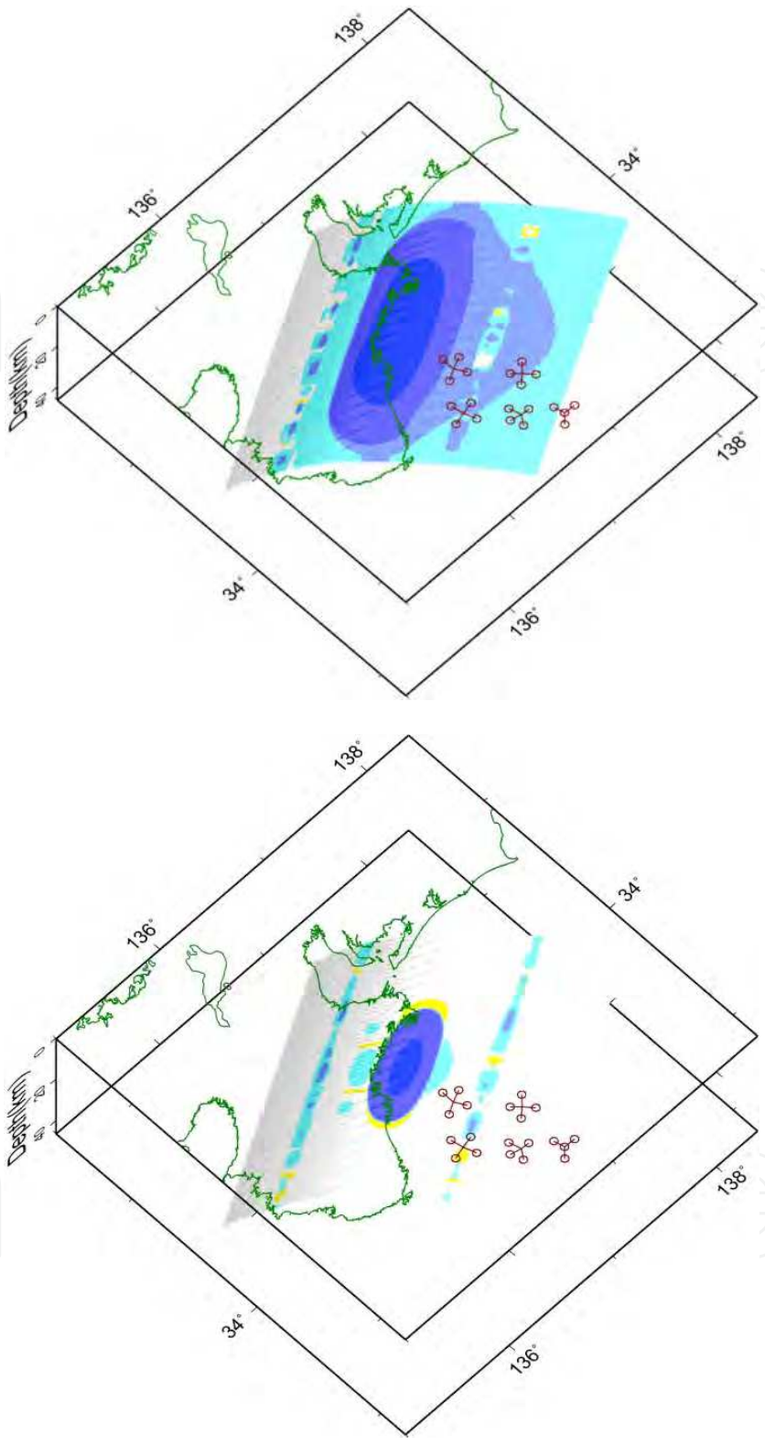

Fig. 12. Snapshots of slip velocity on the plate boundary about 20 years after the megathrust earthquake (top; interseismic period) and 2.5 years before (bottom; preseismic period). Color scale is the same as Fig. 4 but shade effect by applying the command "grdgradient" (Wessel & Smith, 1998) in order to show the bending shape visually. Twenty open circles with five nodes represent observation points of DONET as shown in Fig. 10.

5. Acknowledgment

The authors would like to thank DONET members, Takane Hori and Ryoko Nakata for giving beneficial comments. The authors also would like to thank Tohoku University researchers, Toru Matsuzawa, Ryota Hino and Akira Hasegawa for stimulating our study. J.-P. Ampuero helped us to improve our manuscript with thoughtful discussion. We appreciate publishing managers Igor Babic and Ivana Lorkovic for encouraging our publication, which was partly supported by Grant-in-Aid for Young Scientists (KAKENHI) 23710212.

6. References

Ariyoshi, K.; Matsuzawa, T. & Hasegawa, A. (2007). The key frictional parameters controlling spatial variations in the speed of postseismic-slip propagation on a subduction plate boundary, *Earth Planet. Sci. Lett.*, 256, 136–146, doi:10.1016/j.epsl.2007.01.019.

Ariyoshi, K.; Hori, T.; Ampuero, J.-P.; Kaneda, Y.; Matsuzawa, T.; Hino, R. & Hasegawa, A. (2009). Influence of interaction between small asperities on various types of slow earthquakes in a 3-D simulation for a subduction plate boundary, Gondwana Research, 16(3-4), 534-544, doi: 10.1016/j.gr.2009.03.006.

Ariyoshi, K; Hori, T.; Kaneda, Y.; Ampuero, J.-P.; Matsuzawa, T.; Hino, R. & Hasegawa, A. (2011a). Effects of small asperities on migration of slow-earthquakes along trench direction of subduction plate boundary: investigation through a 3-D numerical simulation, *Adv. in Geosci.*, in press.

Ariyoshi, K; Matsuzawa, T; Ampuero, J.-P.; Nakata, R.; Hori, T.; Kaneda, Y.; Hino, R. & Hasegawa, A. (2011b). Migration process of very low-frequency events based on a chain-reaction model and its application to the detection of preseismic slip for megathrust earthquakes, *Earth Planets Space*, in press.

Blanpied, M. L.; Marone, C. J.; Lockner, D. A.; Byerlee, J. D. & King, D. P. (1998). Quantitative measure of the variation in fault rheology due to fluid-rock interactions, *J. Geophys. Res.*, 103, 9691–9712.

Boatwright, J. & Cocco, M. (1996). Frictional constraints on crustal faulting, *J. Geophys. Res.*, 101, 13895–13909.

Dieterich, J. H. (1979). Modeling of rock friction: 1. Experimental results and constitutive equations, *J. Geophys. Res.*, 84, 2161–2168.

Dragert, H. (2007). Mediating Plate Convergence, *Science*, 315, 471-472, doi: 10.1126/science.1137171.

Hacker, B. R.; Peacock, S. M.; Abers, G. A. & Holloway, S. D. (2003). Subduction factory 2. Are intermediate-depth earthquakes in subducting slabs linked to metamorphic dehydration reactions?, *J. Geophys. Res.*, 108(B1), 2030, doi:10.1029/2001JB001129.

Hirose, H. & Hirahara, K. (2002). A model for complex slip behavior on a large asperity at subduction zones, *Geophysical Research Letters*, 29 (22), 2068.

Hirose, H.; Asano, Y.; Obara, K.; Kimura, T.; Matsuzawa, T.; Tanaka, S. & Maeda, T. (2010). Slow Earthquakes Linked Along Dip in the Nankai Subduction Zone, *Science*, 330(6010), 1502-1502, doi:10.1126/science.1197102.

Ide, S.; Beroza, G. C.; Shelly, D. R. & Uchide, T. (2007). A new scaling law for slow earthquakes, *Nature*, 447, 76–79, doi:10.1038/nature05780.

Kawaguchi, K.; Kaneko, S.; Nishida, T. & Komine, T. (2011). Construction of Real-time Seafloor Observatory for Earthquakes and Tsunami Monitoring, *Praxis book on "Seafloor Observatories"*, in press.

Liu, Y. & Rice, J. R. (2005). Aseismic slip transients emerge spontaneously in three-dimensional rate and state modeling of subduction earthquake sequences, *J. Geophys. Res.*, 110, B08307.

Matsuzawa, T.; Uchida, N.; Igarashi, T.; Okada, T. & Hasegawa, A. (2004). Repeating earthquakes and quasi-static slip on the plate boundary east off northern Honshu, Japan, *Earth Planets Space*, 56, 803–811.

Nakanishi, A.; Kodaira, S.; Miura, S.; Ito, A.; Sato, T.; Park, J.-O.; Kido, Y. & Kaneda, Y. (2008). Detailed structural image around splay-fault branching in the Nankai subduction seismogenic zone: Results from a high-density ocean bottom seismic survey, *J. Geophys. Res.*, 113, B03105.

Nakata, R.; Suda, N. & Tsuruoka, H. (2008). Non-volcanic tremor resulting from the combined effect of Earth tides and slow slip events, *Nature Geosci.*, 1, 676–678, doi:10.1038/ngeo288.

Nadeau, R. M. & Guilhem, A. (2009). Nonvolcanic tremor evolution and the San Simeon and Parkfield, Californinia, Earthquakes, *Science,* 325, 191-193, doi:10.1126/science.1174155.

Obana, K. & Kodaira, S. (2009), Low-frequency tremors associated with reverse faults in a shallow accretionary prism, *Earth Planet. Sci. Lett.*, 287, 168–174, doi:10.1016/j.epsl.2009.08.005.

Obara, K. (2010). Phenomenology of deep slow earthquake family in southwest Japan: Spatiotemporal characteristics and segmentation, *J. Geophys. Res.*, 115, B00A25, doi:10.1029/2008JB006048.

Obara, K. & Shiomi, K. (2009). Underground Structural Anomalies and Slow Earthquake Activities Around Seismogenic Megathrust Earthquake Zone as Revealed by Inland Seismic Observations, *J. Disaster Res.*, 4(2), 83-93.

Okada, Y. (1992). Internal deformation due to shear and tensile faults in a halfspace, *Bull. Seism. Soc. Am.*, 82, 1018–1040.

Rice, J. R. (1993). Spatio-temporal complexity of slip on a fault, *J. Geophys. Res.*, 98, 9885–9907.

Ruina, A. (1983). Slip instability and state variable friction laws, *J. Geophys. Res.*, 88, 10,359–10,370.

Savage, J. C. (1983). A dislocation model of strain accumulation and release at a subduction zone, *J. Geophys. Res.* 88, 4984–4996.

Schwartz, S. Y. & Rokosky, J. M. (2007). Slow slip events and seismic tremor at circum-Pacific subduction zones, *Rev. Geophys.,* vol.45, RC3004, doi:10.1029/2006RG000208.

Shelly, D. R. (2009). Possible deep fault slip preceding the 2004 Parkfield earthquake, inferred from detailed observations of tectonic tremor, *Geophys. Res. Lett.*, 36, L17318, doi:10.1029/2009GL039589.

Shelly, D. R.; Beroza, G. C.; Ide, S. & Nakamura, S. (2006). Low frequency earthquakes in Shikoku, Japan, and their relationship to episodic tremor and slip, *Nature*, 442, 188–191, doi:10.1038/nature04931.

Wang, K. & Suyehiro, K. (1999). How does plate coupling affect crustal stresses in northeast and southwest Japan, *Geophys. Res. Lett.*, 26, 2307–2310, doi:10.1029/1999GL900528.

Wessel, P. & Smith, W. H. F. (1998). New, improved version of the Generic Mapping Tools released, *Eos Trans. AGU*, 79, 579.

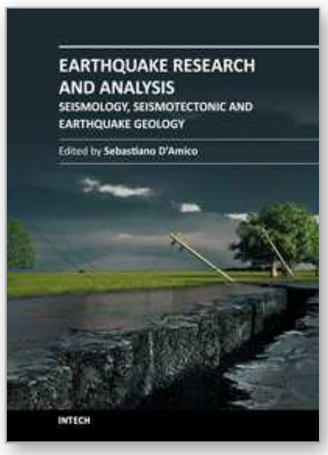

Earthquake Research and Analysis - Seismology, Seismotectonic and Earthquake Geology

Edited by Dr Sebastiano D'Amico

ISBN 978-953-307-991-2
Hard cover, 370 pages
Publisher InTech
Published online 08, February, 2012
Published in print edition February, 2012

This book is devoted to different aspects of earthquake research. Depending on their magnitude and the placement of the hypocenter, earthquakes have the potential to be very destructive. Given that they can cause significant losses and deaths, it is really important to understand the process and the physics of this phenomenon. This book does not focus on a unique problem in earthquake processes, but spans studies on historical earthquakes and seismology in different tectonic environments, to more applied studies on earthquake geology.

How to reference

In order to correctly reference this scholarly work, feel free to copy and paste the following:

Keisuke Ariyoshi and Yoshiyuki Kaneda (2012). Frictional Characteristics in Deeper Part of Seismogenic Transition Zones on a Subduction Plate Boundary, Earthquake Research and Analysis - Seismology, Seismotectonic and Earthquake Geology, Dr Sebastiano D'Amico (Ed.), ISBN: 978-953-307-991-2, InTech, Available from: http://www.intechopen.com/books/earthquake-research-and-analysis-seismology-seismotectonic-and-earthquake-geology/frictional-characteristics-in-deeper-part-of-seismogenic-transition-zone-on-a-subduction-plate-bound

INTECH
open science | open minds

InTech Europe
University Campus STeP Ri
Slavka Krautzeka 83/A
51000 Rijeka, Croatia
Phone: +385 (51) 770 447
Fax: +385 (51) 686 166
www.intechopen.com

InTech China
Unit 405, Office Block, Hotel Equatorial Shanghai
No.65, Yan An Road (West), Shanghai, 200040, China
中国上海市延安西路65号上海国际贵都大饭店办公楼405单元
Phone: +86-21-62489820
Fax: +86-21-62489821

IntechOpen